CARDIOVASCULAR DISEASE

Soft robotic sleeve supports heart function

Ellen T. Roche,[1,2,3] Markus A. Horvath,[1,2,4]* Isaac Wamala,[5]* Ali Alazmani,[1,2,5,6] Sang-Eun Song,[1,2,7] William Whyte,[1,2,8] Zurab Machaidze,[5] Christopher J. Payne,[1,2] James C. Weaver,[2] Gregory Fishbein,[9] Joseph Kuebler,[10] Nikolay V. Vasilyev,[5] David J. Mooney,[1,2] Frank A. Pigula,[5,11†] Conor J. Walsh[1,2†]

There is much interest in form-fitting, low-modulus, implantable devices or soft robots that can mimic or assist in complex biological functions such as the contraction of heart muscle. We present a soft robotic sleeve that is implanted around the heart and actively compresses and twists to act as a cardiac ventricular assist device. The sleeve does not contact blood, obviating the need for anticoagulation therapy or blood thinners, and reduces complications with current ventricular assist devices, such as clotting and infection. Our approach used a biologically inspired design to orient individual contracting elements or actuators in a layered helical and circumferential fashion, mimicking the orientation of the outer two muscle layers of the mammalian heart. The resulting implantable soft robot mimicked the form and function of the native heart, with a stiffness value of the same order of magnitude as that of the heart tissue. We demonstrated feasibility of this soft sleeve device for supporting heart function in a porcine model of acute heart failure. The soft robotic sleeve can be customized to patient-specific needs and may have the potential to act as a bridge to transplant for patients with heart failure.

INTRODUCTION

Traditionally, robots have been used in situations where they do not interact closely with humans—the classical example being assembly lines where metal cages protect factory workers from rigid robots that are capable of applying very high forces. However, the field is being transformed by a new wave of soft robots that are constructed using a combination of elastomers, fibers, and other filler materials. This approach provides opportunities to create robots that are well suited for intimate interactions with humans and with tunable material properties to match biological tissues. Furthermore, through a combination of elegant design and simple control, these soft robots can be programmed to achieve complex motion mimicking the motions of tissues in the human body (*1*–*3*) using specifically designed contractile elements or actuators (*4*–*13*). Previously, the benefit of this approach was shown with extracorporeal robots (*2*, *10*, *14*); however, an exciting opportunity also exists to create implantable soft robotic structures to restore physiological function to, for example, the failing heart.

Heart failure is the inability of the heart to pump sufficient blood to the body, leading to disability or death. Heart failure afflicts 41 million people worldwide including more than 5 million people in the United States (*15*), costing the nation an estimated $32 billion each year (*16*). Currently, patients with end-stage heart failure refractory to medical treatment alone are often considered for heart transplantation. However, donor organ availability is limited, and many patients die awaiting transplantation. To mechanically assist the failing heart, ventricular assist devices (VADs) are used as a life-prolonging therapy, either as a bridge to transplant or, in some cases, as a "destination therapy," meaning the device remains implanted for the rest of the patient's life. Using current VADs, the heart and one or both of the great vessels are cannulated, blood is removed from the heart, and blood is then pumped into the aorta or pulmonary artery. In this scenario, the VAD assumes the function of one or both of the failing ventricles of the heart. The first generation of VADs used a pulsatile pump and valve technology. The second generation of VADs is largely based on a continuous, valveless, axial-flow technology (*17*, *18*), and the third generation uses continuous-flow pumps that use magnetic levitation technology and contactless bearings (*18*).

Although the design improvements implemented with each generation of VADs have helped to reduce prothrombotic components, contact between blood and artificial surfaces remains, necessitating long-term blood-thinning medications for patients with VADs. Despite anticoagulation treatment, the risk of thromboembolic events including stroke may occur in up to 20% of patients (*19*). As outlined in previous work (*20*–*22*), most external devices invert the normal curvature of the heart and act contrary to the remaining native cardiac contraction mechanics, predisposing these devices to reduced biomimicry and efficiency and highlighting an important shortcoming of existing technologies. As a result, many of these devices do not integrate and synchronize with native cardiac contraction mechanics and direction, and some cannot assist the diastolic (filling) phase of the cardiac cycle.

Here, we used soft robotic techniques to develop a tethered implantable sleeve that can provide circulatory support for patients with compromised heart function. The soft robotic sleeve we describe took inspiration from native heart muscle and was designed to augment cardiac function by closely replicating it, instead of disrupting it. Preceding work from our group described the use of soft robotic techniques to replicate the heart's motion (*1*), and here, we present ex vivo and in vivo results in a pig model that builds on this technology to augment heart function.

[1]School of Engineering and Applied Sciences, Harvard University, 29 Oxford Street, Cambridge, MA 02138, USA. [2]Wyss Institute for Biologically Inspired Engineering, 3 Blackfan Circle, Longwood, Boston, MA 02115, USA. [3]Discipline of Biomedical Engineering, College of Engineering and Informatics, National University of Ireland, Galway, Ireland. [4]Technische Universität München, Boltzmannstraße 15, 85748 Garching, Germany. [5]Department of Cardiac Surgery, Boston Children's Hospital, 300 Longwood Avenue, Boston, MA 02115, USA. [6]School of Mechanical Engineering, University of Leeds, Leeds LS2 9JT, U.K. [7]Department of Mechanical and Aerospace Engineering, University of Central Florida, Orlando, FL 32816, USA. [8]Advanced Materials and Bioengineering Research Centre, Royal College of Surgeons in Ireland and Trinity College Dublin, Dublin, Ireland. [9]Department of Anatomic and Clinical Pathology, Ronald Reagan UCLA (University of California, Los Angeles) Medical Center, Los Angeles, CA 90095, USA. [10]Department of Cardiology, Boston Children's Hospital, Boston, MA 02115, USA. [11]Cardiovascular Surgery, School of Medicine, University of Louisville, Louisville, KY 40202, USA.
*Joint second authors.
†Corresponding author. Email: walsh@seas.harvard.edu (C.J.W.); frank.pigula@ulp.org (F.A.P.)

RESULTS

A soft robotic sleeve mimics the material properties and natural motion of the heart

In the heart, complex motion is achieved through the functional arrangement of multiple linear contractile elements oriented spatially in a soft matrix and actuated synergistically. The muscle layers of the heart are arranged in helical and circumferential patterns (*23*–*26*) and simultaneously undergo twisting and compressive motions. The architecture of the native heart was the inspiration for our device, which comprises a fully conformable sleeve with two biomimetic layers of contractile elements embedded in an elastomeric matrix with mechanical properties similar to those of cardiac tissue. Inspired by our previous work on a three-dimensional (3D) structure designed to replicate ventricular twist (*1*), we used a multilayer design to simulate the two outer layers of the myocardial fibers of the heart (Fig. 1, A and B). To create 3D and conformal devices that could be tested in animal models, we exploited fabrication techniques that allowed the integration of custom-designed soft pneumatic artificial muscles (PAMs) into a soft matrix that approximated and conformed to the outer surface of the heart. The PAMs' self-limiting load-length curves (*27*–*29*) provide a physiological, atraumatic strategy to assist and increase native cardiac muscle function. We oriented these PAMs in helical and circumferential patterns, similar to the outer two layers of the myocardial fibers of the heart, to replicate cardiac motion while providing synchronized mechanical assistance.

Two generations of fabrication processes are illustrated in Fig. 1 (C and D), with detailed descriptions in the Supplementary Materials. Briefly, for design 1, a silicone casting process was used to fabricate individual actuators (figs. S1 and S2) and to embed these actuators (Fig. 1C) into a matrix in two separate layers that could be combined, resulting in a device with an overall thickness of 16 mm. Design 2, the final design (Fig. 1D), used a thermoforming process to make the actuators (fig. S3) and combined them into a 2D laminate by selective bonding between thin silicone sheets in a predefined pattern, incorporating circumferentially and helically oriented actuators (referred to as twisting actuators from here on). The resulting device was a thin, flat silicone sleeve about 550 μm thick at the bonded spots between actuators that could be wrapped around the heart and adjusted

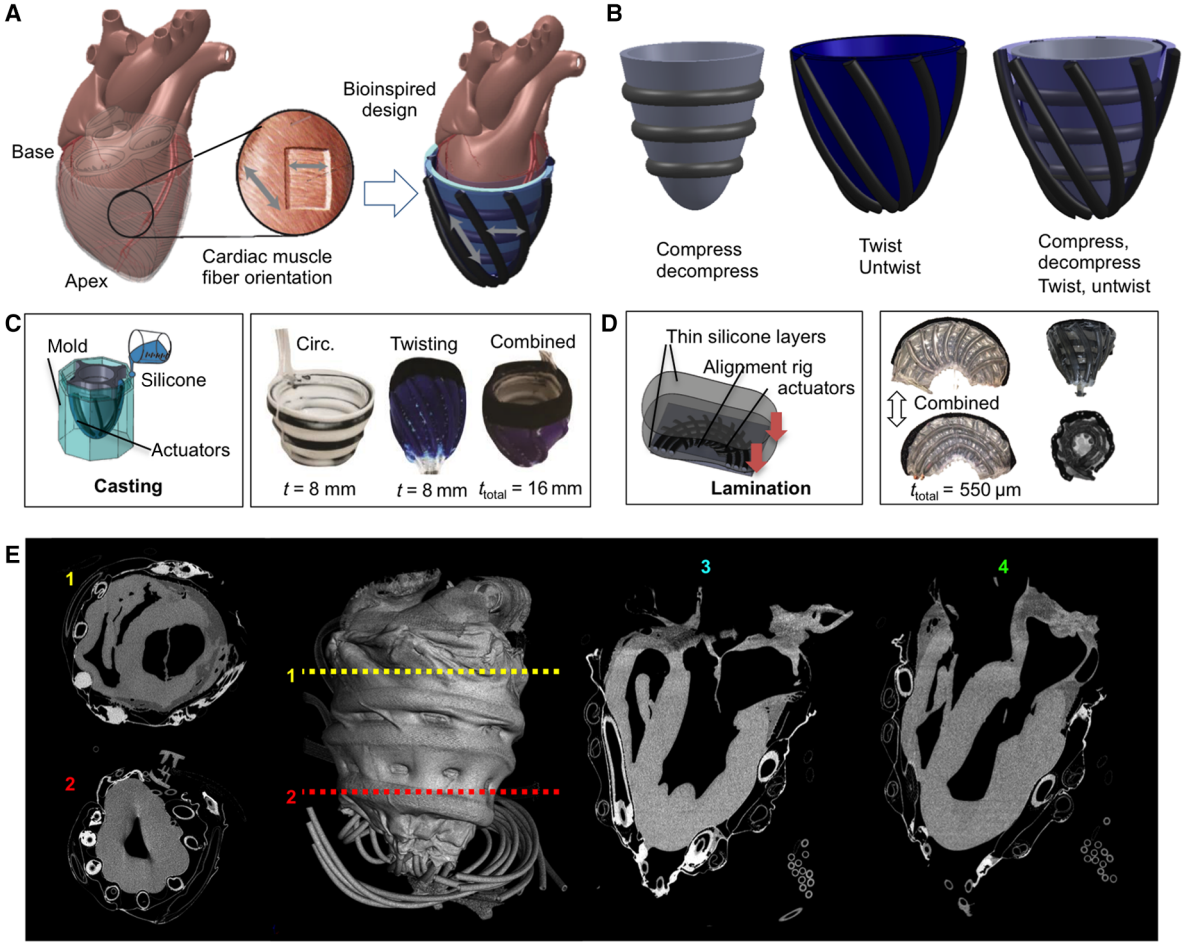

Fig. 1. Design and fabrication of a conformal soft robotic sleeve that can compress and twist. (**A**) The muscle fiber orientations of the outer two layers of the myocardium of the heart inspired the design of the VAD. (**B**) Individual active layers composed of fluidic actuator contractile elements arranged and embedded in soft matrices can compress and decompress, twist and untwist, or simultaneously perform both actions. (**C**) Design 1 was fabricated using a silicone-casting process (shown on the left) to create a bilayer cup-shaped device. Three layers are shown: a circumferential (circ.) layer, a twisting layer, and a combination of circumferential and twisting layers. t, thickness of layer; t_{total}, total thickness of device. (**D**) Design 2 was fabricated by a selective bonding process using a 3D-printed alignment fixture, resulting in a flat monolayer device that can be wrapped around the heart. (**E**) Representative computed tomography images of the posterior view of the heart and transverse (1 and 2) and longitudinal sections (3 and 4) showing both layers of actuators conforming to the heart (design 2).

depending on the size of the heart and the pretensioning required, so that the device could conform to the heart without being overly tight and limiting ventricular filling (*30*). A comparison of the actuator types used in design 1 and design 2 is described in fig. S4 (A to D). Like native heart muscle, the properties of the PAMs are dynamic. The actuators stiffen when pressurized in the systolic phase of the cardiac cycle (fig. S4, E and F). The values for their tensile and compressive moduli when pressurized lie within the ranges of those described for myocardial tissue in the systolic phase (fig. S4, G and H).

The sleeve conforms and couples to the heart surface

Device conformability was determined using computed tomography imaging after wrapping the device around an ex vivo porcine heart filled with saline (Fig. 1E). Sections of the heart demonstrated excellent apposition of the actuators to the epicardial surface (Fig. 1E). A custom-designed flexible sensing sleeve containing an array of pressure sensors colocated with the PAMs could be placed between the epicardium and the device to measure the mechanical interaction between the soft robotic sleeve and heart surface (figs. S5 to S7) (*31*). Ex vivo adhesion testing identified a method combining mesh and chemical fixation at the base of the heart capable of adhering the device to the heart tissue (fig. S8). Dynamic conformity was observed visually and with echocardiography (movie S1).

The soft robotic sleeve synchronizes with native heart motion

One of the main advantages of using soft robotics for cardiac compression is the ability to implement timing schemes to optimize the actuation sequence. A custom control and instrumentation system (Fig. 2A) was developed to program the soft robotic sleeve and to simultaneously monitor and record physiological performance parameters such as heart rate and pulmonary artery and ascending aortic pressure and flow rate. The control system was designed to synchronize with the native cardiac cycle and fine-tune force generation and timing to deliver disease-specific assistance. Two examples of control schemes are depicted in Fig. 2 (B and C), illustrating the triggering of actuation from electrical or hemodynamic parameters of the native cardiac cycle. In Fig. 2B, actuation was triggered from the peak of the QRS complex (R wave) of the electrocardiogram (ECG) trace, and actuators were sequentially pressurized from the apex to the base of the device before sequentially applying vacuum. The time between actuation of individual modules (T1 to T7) could be controlled to allow optimal synchronization with the native cardiac cycle. To allow device triggering before the QRS complex, T1 could also be negative. In Fig. 2C, actuation was triggered from the point of increasing flow rate in the aorta. Any combination of actuators could be pressurized alone, simultaneously, or according to a user-controlled sequence. For example, twisting actuators were pressurized before sequentially pressurizing circumferential actuators (Fig. 2C). Times (T1 to T5) could be controlled from the user interface. Alternatively, circumferential or twisting actuators could be selectively or simultaneously actuated. Right-sided or left-sided actuators could be activated alone or together at the same or different pressures.

The soft robotic sleeve displaces physiological volumes of fluid in an in vitro model

To evaluate the performance of design iterations on a bench-top model in vitro, we fabricated a simplified synthetic heart with one or two ventricles from silicone (Fig. 3A and movie S2). Figure 3 (B to D) shows the results of the in vitro testing. Using a univentricular heart model, volumetric displacements of 38, 22, and 50 ml were achieved for design

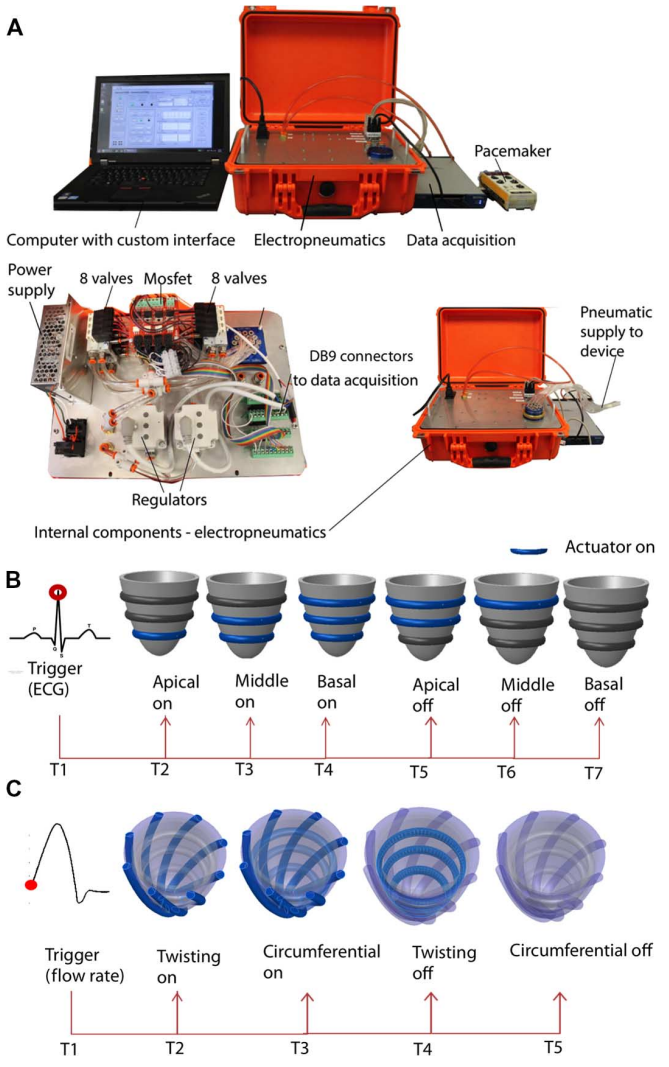

Fig. 2. Hardware components and control system actuation schemes. (**A**) Overview of system with user interface, data acquisition (DAQ) card, electropneumatic control unit, and pacemaker for pacing the heart where necessary. (**B**) Example actuation scheme with trigger from the R peak (red circle) of an ECG trace, and sequential actuation and relaxation from the apex to the base. Time points T1 to T6 can be input by the user by modifying time delays between trigger and valve opening, time between valve opening, and duration of valve opening. Blue color indicates pressurized PAMs (actuation). (**C**) Example actuation scheme triggered from the start of increase of aortic flow (red dot). The twisting actuators are actuated first and then the circumferential. Time points T1 to T5 can be modified by the user from interface. A blue actuator indicates that it is pressurized (on).

1 when the circumferential, twisting, or both layers were actuated, respectively (Fig. 3B). We used design 2 to characterize the effect of externally placing the circumferential or twisting actuator layer with respect to the other actuator layer, that is, whether there was a difference in volumetric displacement dependent on which layer was in close approximation to the model heart. A volumetric displacement of 68 ml was achieved when the twisting actuator layer was placed externally, and 84 ml was displaced when the circumferential actuator layer was placed externally (Fig. 3B) using the univentricular model. As expected, the output increased with pressure (Fig. 3C and movie S2) for design 1 in the univentricular model. In a biventricular model with design 1, higher ejection output was achieved on the left or right

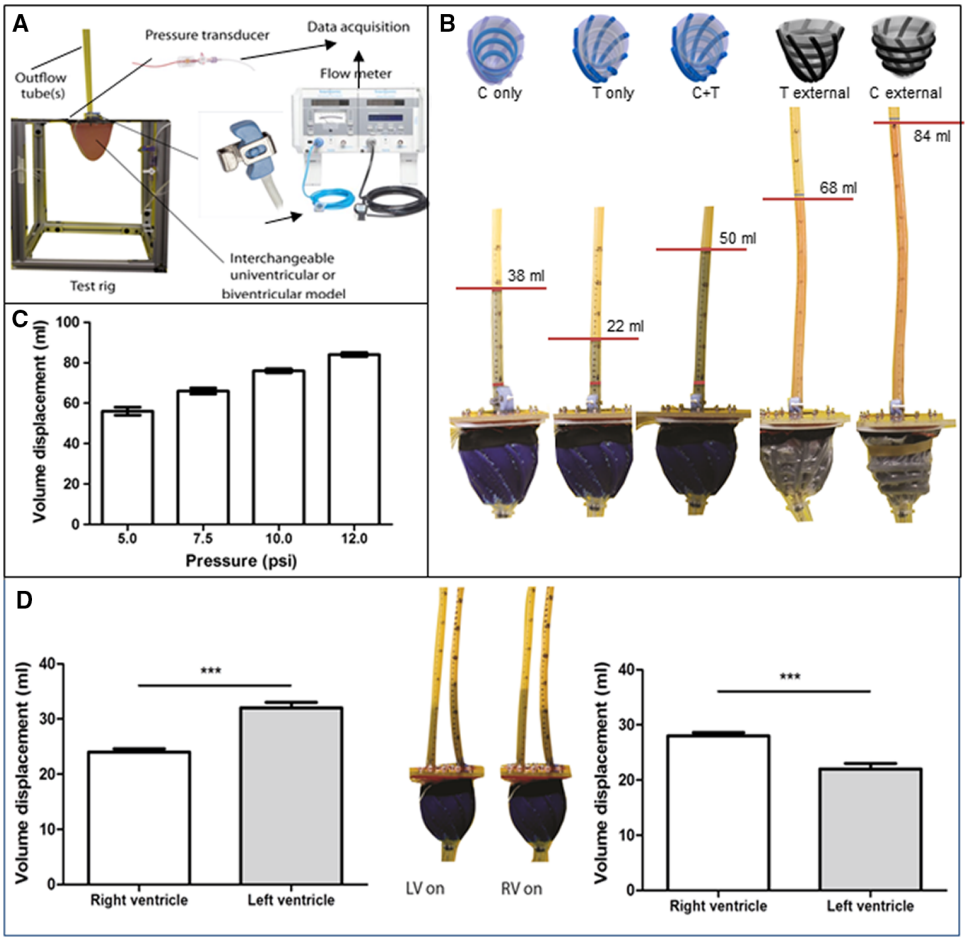

Fig. 3. In vitro testing with a silicone simulator showing volumetric output for a number of conditions. (**A**) The in vitro test setup. A silicone model was mounted onto a test rig, with a latex outflow tube marked with gradations to measure volumetric output. An interventricular pressure transducer measured pressure inside the ventricle. An ultrasonic flow probe was placed on the outflow tube. The model can be exchanged for a univentricular or biventricular model with one or two outflow tubes, respectively. The model was filled with colored water for visualization. (**B**) Models depicting actuation schemes (top) and corresponding images of univentricular volumetric displacements (bottom) measured using circumferential (C) actuators, twisting (T) actuators, twisting and circumferential (C+T) actuators, circumferential actuators inside (T external), and circumferential actuators outside (C external). C, T, and C+T used design 1; T external and C external used design 2. (**C**) Testing with a biventricular model to demonstrate the effect of increasing pressure on output as measured by volume displacement in the test rig setup. (**D**) The effect of selectively actuating left ventricle (LV) or right ventricle (RV) actuators as measured by volume displacement in a biventricular model. Left and right refer to the anatomical left and right of the model, respectively. When the LV actuators were active, there was more output from the left side, and vice versa. Data are means ± SD of $n = 3$; ***$P < 0.001$, *t* test.

side by selectively actuating the circumferential PAMs on the desired side (Fig. 3D and movie S2).

The device increases ejection output in the hearts of pig cadavers

As a first-pass evaluation of control schemes and device positioning for each design, we tested the devices using a fully heparinized porcine model ($n = 2$). Pigs (female adult Yorkshire swine, 60 to 75 kg) were euthanized with sodium pentobarbital before device placement on the heart within the thoracic cavity. We devised a control and data acquisition setup in the operating room to enable recording of aortic blood flow, blood pressure, and ECG and triggering of the device by ECG or pacemaker signal (see Fig. 4A and "In vivo testing" in the Supplementary Materials). A sternotomy was used to open the chest, and the device under evaluation was placed around the heart in the thoracic cavity (Fig. 4, B and C). The ejection output was increased by increasing the actuation pressure (design 1; Fig. 4D). A slightly different waveform for aortic flow could be acquired by varying the actuation pattern (design 1; Fig. 4, E and F, and movie S1). The combined actuation of the circumferential and twisting actuators increased aortic flow more than did either set independently (design 2; Fig. 4, G and H).

The device reestablishes cardiac output in pig hearts during acute asystole in vivo

Although the envisaged use of the device is for augmenting function of the failing heart, we isolated the hemodynamic effect of the device by actuating it on an acutely arrested pig heart, directly after cardiac arrest. A fully heparinized porcine preclinical model was used (female, 60 to 75 kg; $n = 2$ pigs). The device was used to temporarily reestablish cardiac output after drug-induced cardiac arrest. Data were collected for at least 15 min for baseline, asystole, and ventricular assist conditions. Ten representative cycles of aortic flow from each condition were converted to cardiac output per cycle and averaged. Design 1 could achieve ~48% restoration of cardiac output when actuated at its maximum operating pressure of 10 psi at 80 beats per minute (bpm) for a period of 200 ms per cycle (Fig. 5A). Design 2 could achieve ~88% restoration of cardiac output when actuated at its maximum operating pressure of 21 psi at 80 bpm for a period of 200 ms per cycle (Fig. 5B). Representative cycles for baseline function for a healthy adult pig, cardiac asystole, and restoration using ventricular assist are shown in Fig. 5 (A and B), and the average values from 10 representative consecutive cycles are shown in the bar graphs. Movie S3 shows the echocardiographic data from two acutely arrested hearts with the device being active (device on) and passive (device off). The combination of twisting and circumferential actuation resulted in higher aortic flow rates, and thus higher cardiac output, than the independent actuation of either circumferential or twisting elements ($P < 0.001$) (Fig. 5C). Additionally, we compared the aortic flow from the left ventricle and pulmonary flow from the right ventricle while selectively actuating the left side or the right side of the device (Fig. 5, D and E), demonstrating the ability to customize assistance to a specific pathology and actuating one ventricle more than the other.

Inflammation at the device-tissue interface can be modified

To further characterize the effect of device actuation at the device-tissue interface, we conducted histological studies after implanting the device

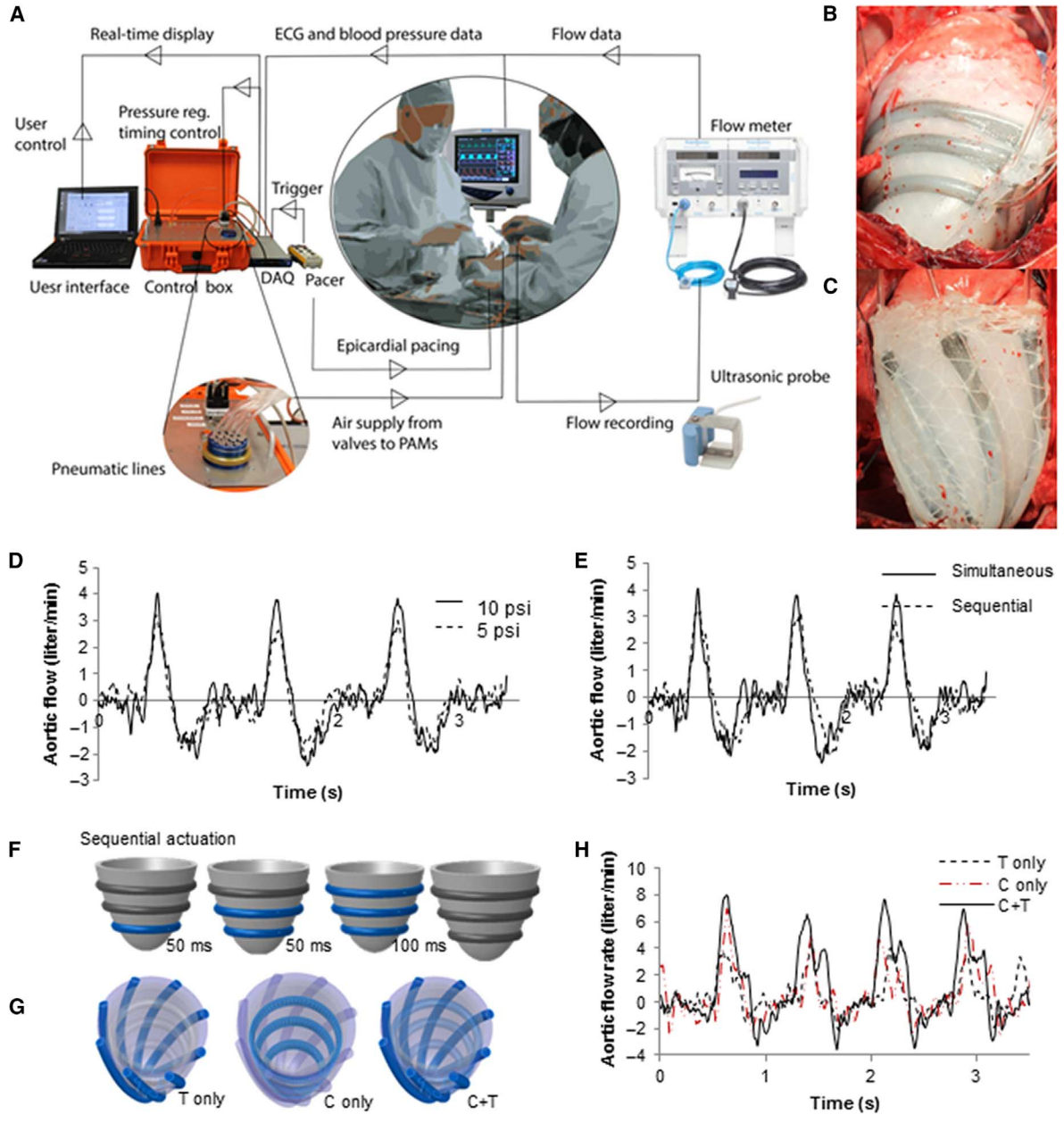

Fig. 4. Testing on porcine cadavers. (**A**) Illustration of setup in the operating room using epicardial pacing. The user interface allows the user to enter the control scheme and control which actuators are active at which time and at what pressure. It also displays the data from the DAQ (ECG, blood pressure, and flow data). If necessary, a pacemaker (pacer) is used to pace the heart epicardially and to trigger the DAQ. A flow meter with ultrasonic probes records flow. Pneumatic lines exit the control box and are connected to each of the actuators in the device, providing air supply from the source through the regulator and valves to the actuators. A PowerLab data acquisition system was used for data collection for later trials. Circumferential (**B**) and twisting (**C**) actuators on a porcine heart. (**D**) Aortic flow when actuated at 5 and 10 psi (design 1). (**E**) Aortic flow when all actuators are simultaneously actuated or sequentially actuated [as described in (F)] (design 1). (**F**) Illustration of example control strategy: sequential actuation of circumferential actuators, starting at the apex. (**G**) Illustration of example control strategy: actuation of twisting (T) only, circumferential (C) only, and both together (C+T). (**H**) Aortic flow rate for twisting, circumferential, and combined actuations (design 2), representative from two trials on $n = 2$ cadaver pigs.

in pigs and rodents in vivo (Fig. 6). Sections of the heart wall were examined after 2 hours of device actuation on an acutely failing heart in the porcine model (Fig. 6A). Sections of the left ventricle, right ventricle, and left atrium showed pronounced infiltration by neutrophils, which was confined to the epicardium, as would be expected after removal of the pericardial fluid and exposure of the heart during surgery (Fig. 6B). The myocardium and endocardium in these areas showed no inflammatory infiltrate or evidence of myocardial injury. There was no epicardial fibrosis or fibrinous exudate, and the coronary arteries appeared normal. On the basis of qualitative assessment, the immune cell infiltrate was no greater in the left ventricle and right ventricle than in the left atrium (the control nonactuated part of the heart), demonstrating that the infiltrate was not attributable to acute device actuation on the heart (fig. S9A). Histological assessment of the apex of the heart, where a U.S. Food and Drug Administration–approved suction device was used for attachment, showed exuberant inflammation through the wall of the

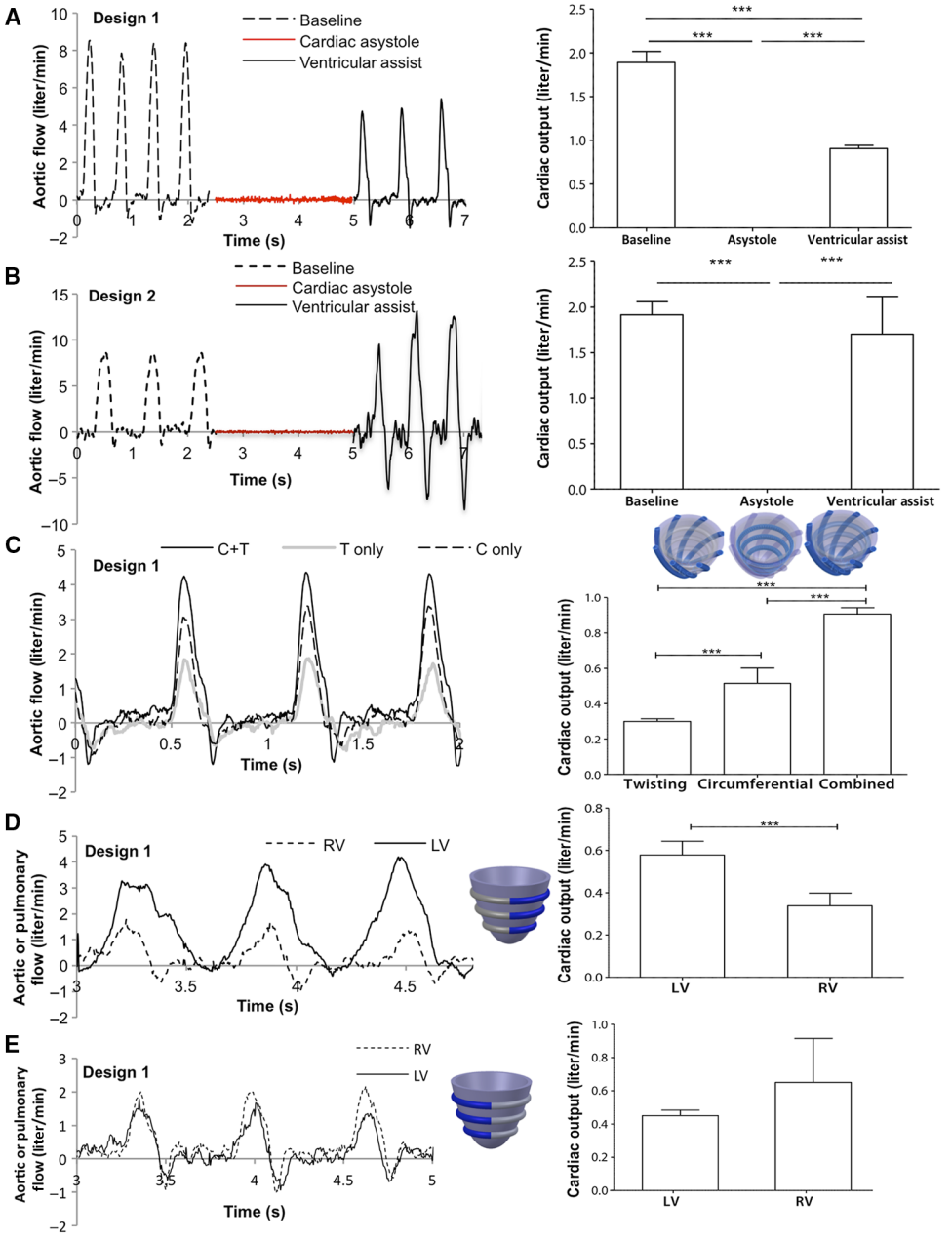

Fig. 5. Device function on porcine heart during acute asystole in vivo. (**A**) Aortic flow and cardiac output for design 1 at a maximum operating pressure of 10 psi at 80 bpm for a period of 200 ms per cycle. Three to four representative cycles are shown for aortic flow; data are means of 10 cardiac cycles + SD for cardiac output. ***$P < 0.001$, one-way analysis of variance (ANOVA) with Tukey's post hoc test. (**B**) Aortic flow and cardiac output for design 2 at a maximum operating pressure of 21 psi at 80 bpm for a period of 200 ms per cycle. Three to four representative cycles are shown for aortic flow; data are means of 10 cardiac cycles + SD for cardiac output. ***$P < 0.001$, one-way ANOVA with Tukey's post hoc test. (**C**) In vivo demonstration of control capabilities for actuation modes described in Fig. 4 (G and H): actuation of twisting (T) only, circumferential (C) only, and both together (C+T) (design 1). Data are means of 10 cardiac cycles + SD. ***$P < 0.001$, one-way ANOVA with Tukey's post hoc test. (**D** and **E**) Aortic (or LV) and pulmonary [or right ventricle (RV)] flow and cardiac output when the left or right side of the device is actuated, respectively (design 1). Aortic or pulmonary flow shows three representative cycles; data are means of 10 cardiac cycles + SD for cardiac output. ***$P < 0.001$, for the right side actuated; $P = 0.1326$, using unpaired t test. Each panel shows representative graph from $n = 2$ animals.

heart (see "apex" image in fig. S9A), motivating the exploration of alternative attachment methods for long-term use of the device.

In anticipation of future chronic device implantation and actuation studies, we developed a hydrogel to use as a protective layer at the device-tissue interface to reduce friction and minimize inflammation when the device is moving over the heart. The hybrid alginate polyacrylamide hydrogel "tough gel" that we used for this purpose was synthesized in a large sheet as previously described (*32*) and has been shown to be nontoxic and biocompatible (*33*). We evaluated the chronic inflammatory effect of the hydrogel material on the epicardial surface of rat hearts implanted with the device for 14 days (Fig. 6C). The hydrogel elicited less of an inflammatory response compared to a control polymer (Fig. 6, D and E), although this reduction was not statistically significant ($P = 0.1$). Finally, we demonstrated in an in vivo porcine model that we could place and actuate the device using the hydrogel at the device-tissue interface (Fig. 6, F and G). The gel did not negatively affect device function (fig. S9B).

The soft robotic sleeve provides cardiac assistance in pigs with acute heart failure

Cardiac assist to the failing heart was demonstrated in six porcine experiments in vivo (Fig. 7A). Acute heart failure was induced in a porcine model by infusing esmolol, a short-acting cardioselective β-blocker that reduced contractility and cardiac output in a dose-dependent fashion, allowing a reproducible induction of heart failure when infused in doses exceeding its therapeutic dose. ECG, blood pressure, and blood flow were recorded after cardiac output had stabilized. Figure 7B shows the results from a representative trial, including the aortic flow rates under three conditions: baseline, acute heart failure, and ventricular assist (three representative cycles for each condition in one animal are shown). Figure 7C shows the average cardiac output for 10 consecutive cycles for each condition in six animals. The cardiac output was reduced to ~45% of baseline when acute heart failure was induced but recovered to ~97% of baseline when active assist was initiated, constituting an augmentation of 113%. The degree of left ventricular twist was quantified in one animal by 3D echocardiography (Fig. 7D) by taking five measurements of twist. The twist decreased in the heart failure condition, but when the device was turned on, the twist was increased to baseline levels ($P = 0.0019$) (Fig. 7D).

To quantify the effect of the soft robotic sleeve on diastolic function of the heart, we used tissue Doppler echocardiography imaging. The

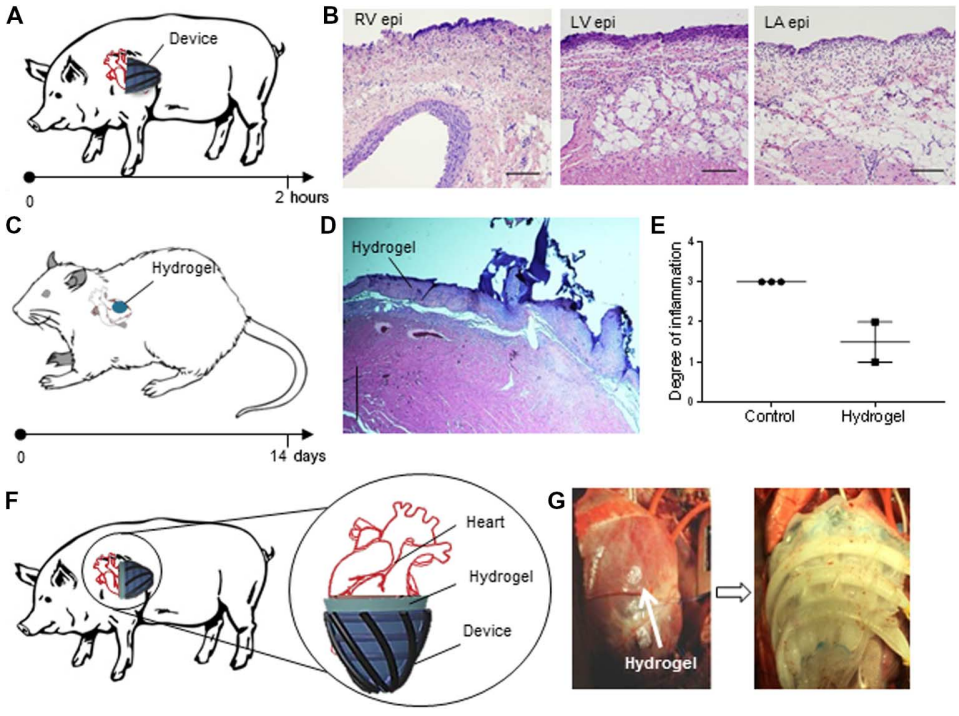

Fig. 6. In vivo assessment of the device-tissue interface and introduction of a hydrogel as a friction-reducing conformable layer. (**A**) Timeline for an acute porcine in vivo study to assess inflammation when the device alone was implanted in contact with the pig heart and actuated for ~2 hours. (**B**) Hematoxylin and eosin (H&E)–stained paraffin-embedded sections of portions of the RV, LV, and left atrium (LA) (control). These are representative images of four sections taken from one animal. Epi, epicardium. Scale bars, 125 μm. (**C**) Timeline for a chronic in vivo rodent study where a hydrogel alone or a urethane polymer (control) was implanted. (**D**) Representative image of H&E-stained paraffin-embedded sections of in vivo rodent heart with hydrogel at 2 weeks after implantation. (**E**) Quantification of the degree of inflammation from the control and hydrogel group. 1, no inflammation; 2, mild inflammation; 3, moderate inflammation; 4, severe inflammation. Ratings are 3 for control ($n = 3$) and 1 and 2 for hydrogel ($n = 2$). Data are median with range; a Mann-Whitney test was used for comparison (not significant, $P = 0.1$). (**F** and **G**) In vivo demonstration of the use of the hydrogel as an intermediate layer at the device-tissue interface in a porcine model (representative of $n = 2$ pigs). The device (white) is placed over the hydrogel in the image on the right.

ratio between early mitral inflow velocity and mitral annular early diastolic velocity (E/e') is a validated method for quantifying diastolic function in clinical practice (*34*). Five measurements were taken with device actuation either in a healthy porcine heart or in a failing porcine heart in vivo using the circumferential actuators, twisting actuators, or both. In the healthy heart, the E/e' ratio was negatively affected by the circumferential actuators but not by the twisting actuators (Fig. 7E). In the failing heart, the contribution of the twisting actuators in restoring the ratio to baseline was greater than that of the circumferential actuators (Fig. 7E).

Although the device is currently tethered to mainline-compressed air supply, the soft robotic sleeve could be used under a greater range of clinical conditions if it was portable. We therefore compared the effects of mains and portable pump power on aortic flow rates in a porcine model under baseline conditions and saw that there was no difference between the two sources (fig. S10, A and B). A schematic of a portable soft robotic sleeve system is shown in fig. S10C, with portable pump and compressed air supplies worn on a belt or backpack, as for current VADs. The cardiac output with the passive device worn on the heart is similar before and after activation (fig. S10, D and E), indicating that the device could be turned off when cardiac assistance is not required. With the active device, femoral pressures were increased in line with aortic pressures (fig. S10F).

DISCUSSION

Here, we introduced a soft robotic sleeve and demonstrated in vivo recovery of cardiac output from a failing heart in a pig model of acute heart failure. About 5.7 million Americans have heart failure (*35*), about half of whom have heart failure with reduced ejection fraction; 5% of this subgroup (~142,500) are in functional New York Heart Association class IV heart failure (*35*). Because there are only about 2100 donor hearts transplanted annually (*36*), there is a clear need for mechanical circulatory support to extend patients' lives. The work described here demonstrated the efficacy of an implantable soft robotic sleeve in assisting the heart, with biomimetic motion and materials that have properties similar to cardiac muscle. This approach would not have been possible with traditional rigid robotic components or with soft materials alone but is possible by leveraging soft robotic technologies to allow programming of customized, conformable materials to dynamically change their stiffness in synchrony with native tissue. Unlike VADs currently in clinical use (*37*), our device restored circulatory function without contacting blood. The soft robotic sleeve, if translated to the clinic, could potentially obviate the need for anticoagulation therapy among patients receiving mechanical circulatory support, thus reducing the risk of complications from clotting, simplifying treatment, and reducing costs. Currently, warfarin, a commonly used blood-thinning medication, requires monitoring of clotting tendency.

Although external cardiac assist devices have been previously explored, many have imposed nonphysiological motions that have failed to mimic the natural motion of the heart, either uniformly squeezing the heart from the outside or using twisting alone to achieve circumferential and longitudinal shortening of the ventricle (*21*, *22*, *38*–*41*). Those devices that twist (*38*–*41*) have not been used preclinically (*39*), report low ejection fractions (*40*), or twist without compressing (*41*). Here, we applied soft manufacturing techniques to make a biomimetic device where actuators could be actuated independently at predefined times and pressures to produce efficient cardiac assistance in synchrony with the failing heart's own inherent, though diminished, motion. Ecoflex 00-30 silicone was selected as the matrix for fabrication of the soft actuated material because it can generate large strains and because its elastic modulus (125 kPa) (*14*) is within the range of reported values for passive myocardial tissue (*42*). Because the PAMs change dynamically, the mechanical properties of the pressurized PAMs (modulus of ~560 kPa) are within the ranges of those described for myocardium in the systolic phase (*43*–*46*). These dynamic material properties are an inherent advantage of our approach because the soft sleeve can mimic the dynamically changing mechanical properties of the native tissue throughout the cardiac cycle. Through this approach, the actuators could restore

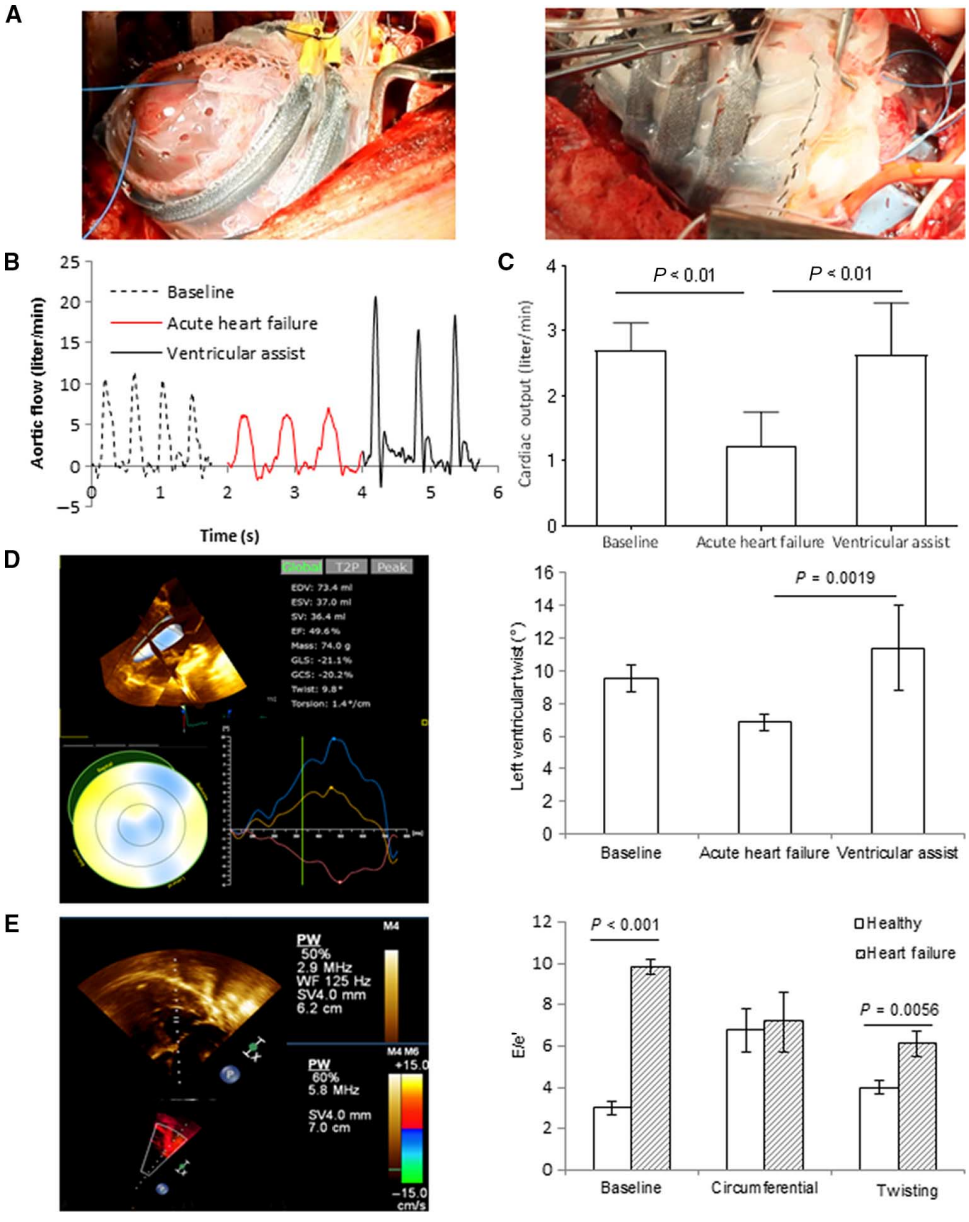

Fig. 7. In vivo demonstration of cardiac assist in a porcine model of acute heart failure. (**A**) Photographic images of the soft robotic sleeve being used as a cardiac assist device on a porcine heart in vivo. (**B** and **C**) Aortic flow of one representative animal under the following conditions: baseline, acute heart failure, and ventricular assist conditions (twisting and circumferential actuators). Three to four representative cycles are shown for each condition. Cardiac output for each condition ($n = 6$ animals). Data are means of 10 cardiac cycles + SD; one-way ANOVA with Tukey's post hoc multiple-comparison test. (**D**) Representative 3D echocardiography (3D echo) image showing left ventricular twist. Five measurements were taken in each condition on one pig. Quantification of left ventricular twist as assessed from 3D echo showing means ± SD; one-way ANOVA with Tukey's post hoc multiple-comparison test. (**E**) Representative 3D echo image showing measurements for the diastolic filling ratio *E*/*e*′ calculation. Five measurements were taken in each condition on one pig. Bar graph shows diastolic filling ratio *E*/*e*′ (means ± SD). Two-way ANOVA for interaction effect. Interaction, $P < 0.0001$; heart failure, $P < 0.0001$; actuation pattern, $P = 0.0003$.

cardiac function along the force vectors of the native heart muscle. We achieved independent or simultaneous compression and twisting as desired through the specific arrangement of the contractile elements and their selective actuation. When pressure was applied to the PAMs, they contracted, and when vacuum was applied, they extended, enabling opposing motions of relaxation (filling) and untwisting. This characteristic of the PAM is critical to providing active device assistance during cardiac diastole, which is an active, energy-dependent biologic process.

Chronic heart failure is characterized by the aberrant motion and remodeling of the failing heart. Growth and repair processes of the heart are guided by mechanical stimuli (*47*, *48*). Remodeling can result in increased ventricle size with dilated, thinned walls. Passive restraint devices and strategies to reduce ventricular size or increase wall thickness have been shown to attenuate or reverse adverse remodeling (*49*–*51*). Our device could potentially be turned off when no longer required, and clinicians could tailor the device as a passive restraint device, partial support, or full support. Thus, the device provides a versatile platform to manipulate the mechanical environment of the heart to target cardiac rehabilitation or recovery. Furthermore, the addition of twisting actuators assisted with the overall function of the heart and contributed to untwisting as well as twisting, which has the potential to assist with diastolic function.

The modularity of the sleeve allows univentricular or biventricular assistance and customization to the needs of the patient. In terms of safety, mechanisms for detecting any leakage or failure of the actuators can be added into the control system, and an individual actuator could be immediately shut off if necessary. The modularity of the design, coupled with the low profile of the passive actuators, allows redundancy (or excess actuators) to be designed in. If one of the actuators fails, and gets deactivated, another "backup" actuator, previously inactive, can take over its function.

The current version of the device is a tethered implantable system and uses wall-compressed air supply for actuation. Further development will need to miniaturize the entire system, so it can be implanted in the body or have the pump and system controller be worn around the waist of the patient, similar to other devices (*18*, *52*, *53*). If a fluidic tether is required to connect an external pump to the soft robotic sleeve, a parallel line could serve as an additional conduit for the delivery of therapeutic agents. Such approach could enable the exciting concept of mechanical biological combination therapy, incorporating reservoirs into the soft robotic sleeve for sustained delivery of small molecules, proteins, or cellular products to promote regeneration or for on-demand antiarrhythmic agents.

Although this study demonstrated proof of concept for this approach, we acknowledge that there are a number of limitations and that further work is required to advance this technology along the translational path. First, the data are from a small number of animals, because the

primary goal of the study was to establish feasibility. Second, the studies were acute and therefore not representative of the remodeling or humoral changes that take place during chronic heart failure. Longer-term implantation studies in animals with chronic heart failure will be required to study the long-term effects of this kind of therapy in vivo including remodeling of the heart and long-term perfusion of end organs by measuring parameters such as lactic acidosis. Third, the biocompatibility of all of the materials should be tested and substituted with appropriate materials if necessary. Fourth, the long-term mechanical properties of the hydrogel interface and the effect of the hydrogel on the long-term efficacy of the device were not investigated. Last, the development of a bioadhesive or biointegrating component will be crucial. Here, we used a combination of mechanical, chemical, and suction strategies for acute device attachment. These approaches would not be adequate for long-term implantation. Ongoing efforts should focus on developing more practical alternatives.

In conclusion, we have demonstrated that a biomimetic soft robotic device, whose material properties and architecture mimic that of the native heart, can support cardiac output in an acutely failing pig heart. By addressing a pressing clinical problem with the application of soft robotic technologies for support of cardiac function, we present an active sleeve that is customizable to patient-specific needs and has a potential to bridge a heart failure patient to transplant or to aid in cardiac rehabilitation and recovery.

MATERIALS AND METHODS

Study design

The overall objective of the study was to demonstrate that our soft robotic sleeve could improve cardiac ejection function. We used a number of in vitro, ex vivo (explanted pig heart), and pig cadaver experiments to optimize the design of the device before proceeding to in vivo pig studies. To test our device in large animals in vivo, an arrested or failing heart swine model was used in $n = 6$ female swine. The study was not blinded or randomized. Cardiac function was assessed in each sow under the following conditions: baseline, heart failure, and device-actuated. Swine were treated with esmolol to induce heart failure. Our heart sleeve device was wrapped around the heart, and aortic flow was measured with an ultrasonic perivascular flow probe on the ascending aorta; data were recorded for 15 min for each condition after stabilization. Ten consecutive cycles for each condition were analyzed and averaged using LabChart software. For the rodent study, Sprague-Dawley female rats were used ($n = 3$ per group). The control group was implanted with a urethane patch on the heart, whereas the experimental group was implanted with alginate polyacrylamide hydrogel on the heart. After 2 weeks, the hearts were explanted and assessed histologically for inflammation. One animal was excluded from the histological analysis because of contamination of the specimen.

Fabrication

All of the fabrication processes are described in detail in the Supplementary Materials. Briefly, actuators were fabricated using either a silicone-casting or thermoplastic-forming process for the internal bladders and placed into an outer mesh. The sleeve with incorporated actuators was manufactured using a silicone-casting process or a selective silicone lamination process. A sensing sleeve was produced using a transfer printing technique.

In vitro testing

The in vitro test setup is illustrated in detail in Fig. 3A. Two model versions were cast from silicone (Ecoflex 00-30) using a 3D-printed mold (Objet Connex 500, Stratasys): a univentricular model and a biventricular model. The base of the model was sealed to an acrylic plate (McMaster-Carr) with a latex outflow tube (McMaster-Carr). The setup was instrumented with a 12-mm flow probe (PS12, Transonics Inc.) on the outflow tube (latex tube with an outer diameter of 16 mm and an inner diameter of 14 mm) connected to a TS402 research console. The outflow tube was marked with a scale to measure volume displacement; the inner diameter of the tubing was 1.6 cm, so each centimeter was equal to a volume of $\pi r^2 h = \pi(0.8)^2(1) = 2.01$ ml. Water used in the model was dyed with food dye (Manta) for visualization.

Ex vivo imaging

Micro–computed tomography imaging was used to visualize the conformation of the device to the heart (X-Tek HMXST225, Nikon Metrology). The following settings were used: a 0.5-mm copper filter, voltage of 120 kV, current of 88 μA, focus of −27, exposure time per image of 5 s, and scan time of 30 min. Reconstruction was carried out with VGStudio MAX and FEI's Avizo 3D software.

Testing on animal cadavers

Female Yorkshire swine ($n = 2$; Parsons Farms) were heparinized [300 IU/kg, intravenously (iv)] after completion of an unrelated in vivo experiment. Sodium pentobarbital (100 mg/kg; Fatal-Plus, Vortex Pharmaceuticals) was used for euthanasia, and the animal was mechanically ventilated immediately after sacrifice, so that lung inflation and deflation would be representative of a surgical situation. Flow in the aorta was recorded with a Transonics flow probe (AD Instruments), and data were recorded as described in Fig. 4A.

In vivo porcine studies

All animals received humane care in accordance with the 1996 *Guide for the Care and Use of Laboratory Animals* recommended by the U.S. National Institutes of Health. The acute porcine studies were performed at the Boston Children's Hospital, and the experimental protocol was approved by the hospital's Institutional Animal Care and Use Committee. Female Yorkshire swine ($n = 6$; Parsons Farms) with a body weight of 60 to 75 kg were used. Anesthesia induction and maintenance are described in the Supplementary Materials. A sternotomy was used to access the chest for device and instrumentation placement. Cardiac output was quantified by directly measuring blood output from the heart using perivascular flow probes (Transonics TS420) at the aorta. For the acute asystole experiments, cardiac arrest was induced using sodium pentobarbital (Vortex Pharmaceuticals). Before arrest, the pigs were heparinized (300 IU/kg, iv; Hospira) and baselines were recorded. Flows were recorded after cardiac arrest, followed by device placement and actuation at several experimental parameters. For the acute heart failure studies, esmolol (Mylan) was infused at a rate of 0.15 to 1 mg kg^{-1} min^{-1} and supplemented by bolus injections of 0.5 to 1 mg/kg as needed to achieve a decrease of at least 50% in cardiac output. The device was synchronized to the heart by pacing both the ventricles and the device using a dual chamber pacemaker (5342, Medtronic Inc.). A delay could be fine-tuned manually so that the device was activated at any chosen time period before or after the pacemaker signal to the heart. All data were logged continuously in real time using the LabChart data logger (AD Instruments). For the acute inflammation test, samples ($n = 3$) were taken from the ventricles, atria, and apex of the heart for histological assessment. After paraffin embedding and sectioning, eight heart sections from each animal were stained with H&E and examined microscopically by a cardiovascular pathologist. 3D echocardiography and speckle studies were performed by a cardiol-

ogist who specializes in imaging using an iE33 ultrasound machine (Philips) with an x7-2 transducer probe (Philips).

In vivo rodent studies

The in vivo rodent experiments were conducted at Harvard University and were approved by the Harvard University Institutional Animal Care and Use Committee. Sprague-Dawley female rats ($n = 3$ per group and $n = 2$ for suture group due to contamination of specimen) (200 to 225 g) were used. Alginate polyacrylamide hydrogel (5 mm in diameter, 1-mm-thick disc), manufactured as previously described (*33*), or a control urethane polymer (5 mm in diameter, 0.2-mm-thick disc), fabricated as previously described (*54*), was placed on the left ventricle of the heart and secured with one suture via a minithoracotomy as previously described (*55*). Animals were assessed after 2 weeks, at which point tissue samples were taken from the ventricles for histological assessment. After fixing, paraffin embedding, and sectioning, tissue samples were stained with H&E and examined microscopically by a histopathology expert. Two to four representative sections were examined per animal.

Statistics

LabChart Pro (AD Instruments) was used for data analysis. Comments were added to the scope view during the trial. Ten representative cycles for each condition were analyzed. The value for cardiac output was calculated by recording both the aortic and pulmonary flow at 0.005-s intervals and then averaging the cardiac output for each of the 10 consecutive representative cycles. SDs are representative of cycle-to-cycle variations. Normality tests were carried out using histograms. For normally distributed data, a two-sided, unpaired t test was used for comparing between two groups, with an α level of 0.05. A one-way ANOVA with Tukey's post hoc test was used for groups of more than two, with an α level of 0.05. For data that were not normally distributed, a Mann-Whitney test was used to compare between two groups. A two-way ANOVA was used for grouped multiple-comparison analysis of E/e'. Additionally, in this group, statistics between healthy pig heart and a pig heart during acute failure were determined using the Bonferroni-Dunn method without assuming a consistent SD.

SUPPLEMENTARY MATERIALS

www.sciencetranslationalmedicine.org/cgi/content/full/9/373/eaaf3925/DC1
Materials and Methods
Fig. S1. The operation of a McKibben actuator.
Fig. S2. Fabrication of PAMs with silicone bladders.
Fig. S3. Forming of thermoplastic urethane balloons.
Fig. S4. A comparison of silicone and thermoplastic urethane actuators and dynamic material properties of the actuators.
Fig. S5. Sensor fabrication.
Fig. S6. Sensing sleeve fabrication.
Fig. S7. Sensing sleeve realization.
Fig. S8. Adhesion testing.
Fig. S9. Histology from the heart after acute device use and demonstration that hydrogel interface does not affect device function.
Fig. S10. Portable power for the device, turning the device off, and peripheral perfusion in a porcine model.
Movie S1. Demonstration of device conformability and control scheme.
Movie S2. In vitro testing.
Movie S3. Echocardiographic data.
References (*56*, *57*)

REFERENCES AND NOTES

1. E. T. Roche, R. Wohlfarth, J. T. B. Overvelde, N. V. Vasilyev, F. A. Pigula, D. J. Mooney, K. Bertoldi, C. J. Walsh, A bioinspired soft actuated material. *Adv. Mater.* **26**, 1200–1206 (2014).
2. P. Polygerinos, Z. Wang, K. C. Galloway, R. J. Wood, C. J. Walsh, Soft robotic glove for combined assistance and at-home rehabilitation. *Rob. Auton. Syst.* **73**, 135–143 (2015).
3. R. Deimel, O. Brock, A novel type of compliant and underactuated robotic hand for dexterous grasping. *Int. J. Rob. Res.* **35**, 161–185 (2016).
4. F. Ilievski, A. D. Mazzeo, R. F. Shepherd, X. Chen, G. M. Whitesides, Soft robotics for chemists. *Angew. Chem. Int. Ed. Engl.* **50**, 1890–1895 (2011).
5. R. V. Martinez, J. L. Branch, C. R. Fish, L. Jin, R. F. Shepherd, R. M. D. Nunes, Z. Suo, G. M. Whitesides, Robotic tentacles with three-dimensional mobility based on flexible elastomers. *Adv. Mater.* **25**, 205–212 (2013).
6. R. V. Martinez, C. R. Fish, X. Chen, G. M. Whitesides, Elastomeric origami: Programmable paper-elastomer composites as pneumatic actuators. *Adv. Funct. Mater.* **22**, 1376–1384 (2012).
7. R. F. Shepherd, F. Ilievski, W. Choi, S. A. Morin, A. A. Stokes, A. D. Mazzeo, X. Chen, M. Wang, G. M. Whitesides, Multigait soft robot. *Proc. Natl. Acad. Sci. U.S.A.* **108**, 20400–20403 (2011).
8. K. Suzumori, T. Maeda, H. Watanabe, T. Hisada, Fiberless flexible microactuator designed by finite-element method. *IEEE ASME Trans. Mechatron.* **2**, 281–286 (1997).
9. K. Suzumori, S. Endo, T. Kanda, N. Kato, H. Suzuki, A bending pneumatic rubber actuator realizing soft-bodied manta swimming robot, in *IEEE Conference on Robotics and Automation* (IEEE, 2007), pp. 4975–4980.
10. B. Mazzolai, L. Margheri, M. Cianchetti, P. Dario, C. Laschi, Soft-robotic arm inspired by the octopus: II. From artificial requirements to innovative technological solutions. *Bioinspir. Biomim.* **7**, 025005 (2012).
11. A. D. Marchese, C. D. Onal, D. Rus, Autonomous soft robotic fish capable of escape maneuvers using fluidic elastomer actuators. *Soft Robot.* **1**, 75–87 (2014).
12. C. D. Onal, D. Rus, Autonomous undulatory serpentine locomotion utilizing body dynamics of a fluidic soft robot. *Bioinspir. Biomim.* **8**, 026003 (2013).
13. K. Jung, J. C. Koo, J.-d. Nam, Y. K. Lee, H. R. Choi, Artificial annelid robot driven by soft actuators. *Bioinspir. Biomim.* **2**, S42–S49 (2007).
14. Y.-L. Park, B.-r. Chen, D. Young, L. Stirling, R. J. Wood, E. Goldfield, R. Nagpal, Bio-inspired active soft orthotic device for ankle foot pathologies. *IEEE/RSJ Int. Conf. Intell. Robot. Syst.* **2011**, 4488–4495 (2011).
15. A. S. Go, D. Mozaffarian, V. L. Roger, E. J. Benjamin, J. D. Berry, W. B. Borden, D. M. Bravata, S. Dai, E. S. Ford, C. S. Fox, S. Franco, H. J. Fullerton, C. Gillespie, S. M. Hailpern, J. A. Heit, V. J. Howard, M. D. Huffman, B. M. Kissela, S. J. Kittner, D. T. Lackland, J. H. Lichtman, L. D. Lisabeth, D. Magid, G. M. Marcus, A. Marelli, D. B. Matchar, D. K. McGuire, E. R. Mohler, C. S. Moy, M. E. Mussolino, G. Nichol, N. P. Paynter, P. J. Schreiner, P. D. Sorlie, J. Stein, T. N. Turan, S. S. Virani, N. D. Wong, D. Woo, M. B. Turner, Heart disease and stroke statistics—2013 update: A report from the American Heart Association. *Circulation* **127**, e6–e245 (2013).
16. P. A. Heidenreich, J. G. Trogdon, O. A. Khavjou, J. Butler, K. Dracup, M. D. Ezekowitz, E. A. Finkelstein, Y. Hong, S. C. Johnston, A. Khera, D. M. Lloyd-Jones, S. A. Nelson, G. Nichol, D. Orenstein, P. W. F. Wilson, Y. J. Woo, Forecasting the future of cardiovascular disease in the United States: A policy statement from the American Heart Association. *Circulation* **123**, 933–944 (2011).
17. M. M. Givertz, Ventricular assist devices: Important information for patients and families. *Circulation* **124**, e305–e311 (2011).
18. L. E. Rodriguez, E. E. Suarez, M. Loebe, B. A. Bruckner, Ventricular assist devices (VAD) therapy: New technology, new hope? *Methodist Debakey Cardiovasc. J.* **9**, 32–37 (2013).
19. M. Shahinpoor, A review of patents on implantable heart-compression/assist devices and systems. *Recent Pat. Biomed. Eng.* **3**, 54–71 (2010).
20. M. R. Moreno, S. Biswas, L. D. Harrison, G. Pernelle, M. W. Miller, T. W. Fossum, D. A. Nelson, J. C. Criscione, Assessment of minimally invasive device that provides simultaneous adjustable cardiac support and active synchronous assist in an acute heart failure model. *J. Med. Devices* **5**, 41008-1–41008-9 (2011).
21. M. R. Moreno, S. Biswas, L. D. Harrison, G. Pernelle, M. W. Miller, T. W. Fossum, D. A. Nelson, J. C. Criscione, Development of a non-blood contacting cardiac assist and support device: An in vivo proof of concept study. *J. Med. Devices* **5**, 41007-1–41007-9 (2011).
22. M. C. Oz, J. H. Artrip, D. Burkhoff, Direct cardiac compression devices. *J. Heart Lung Transplant.* **21**, 1049–1055 (2002).
23. G. D. Buckberg, Basic science review: The helix and the heart. *J. Thorac. Cardiovasc. Surg.* **124**, 863–883 (2002).
24. G. Buckberg, J. I. E. Hoffman, A. Mahajan, S. Saleh, C. Coghlan, Cardiac mechanics revisited: The relationship of cardiac architecture to ventricular function. *Circulation* **118**, 2571–2587 (2008).
25. P. P. Sengupta, B. K. Khandheria, J. Narula, Twist and untwist mechanics of the left ventricle. *Heart Fail. Clin.* **4**, 315–324 (2008).
26. P. P. Sengupta, J. Korinek, M. Belohlavek, J. Narula, M. A. Vannan, A. Jahangir, B. K. Khandheria, Left ventricular structure and function: Basic science for cardiac imaging. *J. Am. Coll. Cardiol.* **48**, 1988–2001 (2006).

27. G. K. Klute, J. M. Czerniecki, B. Hannaford, Proceedings of the 1999 IEEE/ASME International Conference on Advanced Intelligent Mechatronics, Atlanta, Georgia, 19 to 23 September 1999.
28. C.-P. Chou, B. Hannaford, Static and dynamic characteristics of McKibben pneumatic artificial muscles. *IEEE Conf. Robot. Autom.* **1**, 281–286 (1994).
29. S. C. Obiajulu, E. T. Roche, F. A. Pigula, C. J. Walsh, Proceedings of the ASME 2013 International Design Engineering Technical Conferences & Computers and Information in Engineering Conference, Portland, OR, 4 to 7 August 2013.
30. E. T. Roche, M. A. Horvath, A. Alazmani, K. C. Galloway, N. V. Vasilyev, D. J. Mooney, F. A. Pigula, C. J. Walsh, Design and fabrication of a soft robotic direct cardiac assist device, in Proceedings of the ASME 2015 International Design Engineering Technical Conferences & Computers and Information in Engineering Conference IDETC/CIE, Boston, Massachusetts, 2 to 5 August 2015.
31. M. A. Horvath, E. T. Roche, D. M. Vogt, D. J. Mooney, F. A. Pigula, C. J. Walsh, Soft pressure sensing sleeve for direct cardiac compression device, in Proceedings of the ASME 2015 International Design Engineering Technical Conferences & Computers and Information in Engineering Conference IDETC/CIE, Boston, Massachusetts, 2 to 5 August 2015.
32. J.-Y. Sun, X. Zhao, W. R. K. Illeperuma, O. Chaudhuri, K. H. Oh, D. J. Mooney, J. J. Vlassak, Z. Suo, Highly stretchable and tough hydrogels. *Nature* **489**, 133–136 (2012).
33. M. C. Darnell, J.-Y. Sun, M. Mehta, C. Johnson, P. R. Arany, Z. Suo, D. J. Mooney, Performance and biocompatibility of extremely tough alginate/polyacrylamide hydrogels. *Biomaterials* **34**, 8042–8048 (2013).
34. J.-H. Park, T. H. Marwick, Use and limitations of E/e' to assess left ventricular filling pressure by echocardiography. *J. Cardiovasc. Ultrasound* **19**, 169–173 (2011).
35. Writing Group Members, D. Mozaffarian, E. J. Benjamin, A. S. Go, D. K. Arnett, M. J. Blaha, M. Cushman, S. R. Das, S. de Ferranti, J.-P. Després, H. J. Fullerton, V. J. Howard, M. D. Huffman, C. R. Isasi, M. C. Jiménez, S. E. Judd, B. M. Kissela, J. H. Lichtman, L. D. Lisabeth, S. Liu, R. H. Mackey, D. J. Magid, D. K. McGuire, E. R. Mohler III, C. S. Moy, P. Muntner, M. E. Mussolino, K. Nasir, R. W. Neumar, G. Nichol, L. Palaniappan, D. K. Pandey, M. J. Reeves, C. J. Rodriguez, W. Rosamond, P. D. Sorlie, J. Stein, A. Towfighi, T. N. Turan, S. S. Virani, D. Woo, R. W. Yeh, M. B. Turner; American Heart Association Statistics Committee; Stroke Statistics Subcommittee, Heart disease and stroke statistics—2016 update: A report from the American Heart Association. *Circulation* **133**, e38–e360 (2016).
36. J. K. Patel, J. A. Kobashigawa, Heart transplantation. *Circulation* **124**, e132–e134 (2011).
37. D. Mancini, P. C. Colombo, Left ventricular assist devices: A rapidly evolving alternative to transplant. *J. Am. Coll. Cardiol.* **65**, 2542–2555 (2015).
38. US Patent US8075471, D. R. Trumble, Apical torsion device for cardiac assist (2011).
39. US Patent US20090131740, M. Gharib, Cardiac assist system using helical arrangement of contractile bands and helically-twisting cardiac assist device (2009).
40. P. Tozzi, A. Michalis, D. Hayoz, D. Locca, L. K. von Segesser, Artificial muscle for end-stage heart failure. *ASAIO J.* **58**, 103–108 (2012).
41. D. R. Trumble, W. E. McGregor, R. C. P. Kerckhoffs, L. K. Waldman, Cardiac assist with a twist: Apical torsion as a means to improve failing heart function. *J. Biomech. Eng.* **133**, 101003-1–101003-10 (2011).
42. T. Shishido, M. Sugimachi, O. Kawaguchi, H. Miyano, T. Kawada, W. Matsuura, Y. Ikeda, T. Sato, J Alexander Jr., K. Sunagawa, A new method to measure regional myocardial time-varying elastance using minute vibration. *Am. J. Physiol.* **274**, H1404–H1415 (1998).
43. A. I. Hassaballah, M. A. Hassan, A. N. Mardi, M. Hamdi, An inverse finite element method for determining the tissue compressibility of human left ventricular wall during the cardiac cycle. *PLOS ONE* **8**, e82703 (2013).
44. J. Shim, A. Grosberg, J. C. Nawroth, K. K. Parker, K. Bertoldi, Modeling of cardiac muscle thin films: Pre-stretch, passive and active behavior. *J. Biomech.* **45**, 832–841 (2012).
45. F. Dorri, P. F. Niederer, P. P. Lunkenheimer, A finite element model of the human left ventricular systole. *Comput. Methods Biomech. Biomed. Engin.* **9**, 319–341 (2006).
46. S. Marchesseau, H. Delingette, M. Sermesant, M. Sorine, K. Rhode, S. G. Duckett, C. A. Rinaldi, R. Razavi, N. Ayache, Preliminary specificity study of the Bestel–Clément–Sorine electromechanical model of the heart using parameter calibration from medical images. *J. Mech. Behav. Biomed. Mater.* **20**, 259–271 (2013).
47. P. Patwari, R. T. Lee, Mechanical control of tissue morphogenesis. *Circ. Res.* **103**, 234–243 (2008).
48. L. A. Taber, Biomechanics of cardiovascular development. *Annu. Rev. Biomed. Eng.* **3**, 1–25 (2001).
49. P. A. Chaudhry, T. Mishima, V. G. Sharov, J. Hawkins, C. Alferness, G. Paone, H. N. Sabbah, Passive epicardial containment prevents ventricular remodeling in heart failure. *Ann. Thorac. Surg.* **70**, 1275–1280 (2000).
50. US Patent US6224540, D. M. Lederman, R. T. V. Kung, Passive girdle for heart ventricle for therapeutic aid to patients having ventricular dilatation (2001).
51. M. Taramasso, M. De Bonis, E. Lapenna, A. Verzini, G. La Canna, A. Grimaldi, O. Alfieri, Reverse remodeling effect of the CorCap despite the presence of severe mitral regurgitation. *Ann. Thorac. Surg.* **87**, e23–e24 (2009).
52. C. A. Thunberg, B. D. Gaitan, F. A. Arabia, D. J. Cole, A. M. Grigore, Ventricular assist devices today and tomorrow. *J. Cardiothorac. Vasc. Anesth.* **24**, 656–680 (2010).
53. S. Kyo, S. Takamoto, Ventricular assist device. *Kyobu Geka* **62**, 704–711 (2009).
54. E. T. Roche, A. Fabozzo, Y. Lee, P. Polygerinos, I. Friehs, L. Schuster, W. Whyte, A. M. Casar Berazaluce, A. Bueno, N. Lang, M. J. N. Pereira, E. Feins, S. Wasserman, E. D. O'Cearbhaill, N. V. Vasilyev, D. J. Mooney, J. M. Karp, P. J. del Nido, C. J. Walsh, A light-reflecting balloon catheter for atraumatic tissue defect repair. *Sci. Transl. Med.* **7**, 306ra149 (2015).
55. E. T. Roche, C. L. Hastings, S. A. Lewin, D. E. Shvartsman, Y. Brudno, N. V. Vasilyev, F. J. O'Brien, C. J. Walsh, G. P. Duffy, D. J. Mooney, Comparison of biomaterial delivery vehicles for improving acute retention of stem cells in the infarcted heart. *Biomaterials* **35**, 6850–6858 (2014).
56. F. Daerden, D. Lefeber, Pneumatic artificial muscles: Actuators for robotics and automation. *Eur. J. Mech. Environ. Eng.* **47**, 10–21 (2000).
57. G. Andrikopoulos, G. Nikolakopoulos, S. Manesis, A survey on applications of pneumatic artificial muscles, in 19th Mediterranean Conference on Control and Automation, Corfu, Greece, 20 to 23 June 2011.

Acknowledgments: We thank the Wyss Institute and the School of Engineering and Applied Sciences. We thank the Animal Research Children's Hospital staff at Boston Children's Hospital for their support and assistance in this project. We acknowledge J. Li for assistance with the rodent in vivo study. **Funding:** This study was supported by a Translational Research Program grant from Boston Children's Hospital and a Director's Challenge Cross-Platform grant from the Wyss Institute for Biologically Inspired Engineering, Harvard School of Engineering and Applied Sciences. This study was also supported by the Science Foundation Ireland under grant number 12/RC/2278 (to W.W.). **Author contributions:** E.T.R., M.A.H., A.A., and I.W. designed and fabricated the devices. A.A. and S.-E.S. designed the control system and software. E.T.R. and M.A.H. characterized the actuators. E.T.R., M.A.H., I.W., A.A., W.W., S.-E.S., C.J.P., N.V.V., J.K., G.F., and Z.M. conducted the porcine studies. E.T.R., A.A., D.J.M., N.V.V., F.A.P., and C.J.W. designed the research. E.T.R., M.A.H., I.W., A.A., W.W., S.-E.S., C.J.P., N.V.V., Z.M., and F.A.P. performed in vitro studies. W.W. fabricated the hydrogel liner. J.C.W. and I.W. performed computed tomography imaging. E.R. and W.W. conducted the rodent studies. J.K. and G.F. conducted imaging and analysis for twist and diastolic measurements. E.T.R., M.A.H., I.W., A.A., W.W., J.C.W., J.K., and G.F. analyzed the data. E.T.R., M.A.H., I.W., C.J.P., D.J.M., F.A.P., and C.J.W. wrote the paper. **Competing interests:** E.T.R, D.J.M., F.A.P., and C.J.W. are authors on a patent application 15/027,246, "Biomimetic actuation device and system, and methods for controlling a biomimetic actuation device and system," submitted by Harvard University, which covers design and manufacturing methods for the actuators, device, and control system. **Data and materials availability:** All data reported in the paper are included in the manuscript or available in the Supplementary Materials. Requests for materials should be addressed to C.J.W. (walsh@seas.harvard.edu) and will be handled according to a material transfer agreement through Harvard University.

Submitted 3 February 2016
Accepted 23 December 2016
Published 18 January 2017
10.1126/scitranslmed.aaf3925

Citation: E. T. Roche, M. A. Horvath, I. Wamala, A. Alazmani, S.-E. Song, W. Whyte, Z. Machaidze, C. J. Payne, J. C. Weaver, G. Fishbein, J. Kuebler, N. V. Vasilyev, D. J. Mooney, F. A. Pigula, C. J. Walsh, Soft robotic sleeve supports heart function. *Sci. Transl. Med.* **9**, eaaf3925 (2017).

Science Translational Medicine
AAAS

Soft robotic sleeve supports heart function

Ellen T. Roche, Markus A. Horvath, Isaac Wamala, Ali Alazmani, Sang-Eun Song, William Whyte, Zurab Machaidze, Christopher J. Payne, James C. Weaver, Gregory Fishbein, Joseph Kuebler, Nikolay V. Vasilyev, David J. Mooney, Frank A. Pigula and Conor J. Walsh (January 18, 2017)

Science Translational Medicine **9** (373), . [doi: 10.1126/scitranslmed.aaf3925]

Editor's Summary

Robots have a change of heart

Ventricular assist devices help failing hearts function by pumping blood but require monitoring and anticoagulant therapy to prevent blood clot formation. Roche *et al*. created a soft robotic device with material properties similar to those of native heart tissue that sits snugly around the heart and provides ventricular assistance without ever contacting blood. The robotic sleeve uses compressed air to power artificial silicone muscles that compress and twist, mimicking the movements of the normal human heart. The authors show that the artificial muscles could be selectively activated to twist, compress, or simultaneously perform both actions on one side or both sides of the heart. The device increased cardiac ejection volume in vitro and when implanted in adult pigs during drug-induced cardiac arrest.

Science Translational Medicine (print ISSN 1946-6234; online ISSN 1946-6242) is published weekly, except the last week in December, by the American Association for the Advancement of Science, 1200 New York Avenue, NW, Washington, DC 20005.